

RESEARCH ARTICLE | JULY 20 2020

**Frequency-dependent response in cortical network with periodic electrical stimulation** Special Collection: [Dynamical Disease: A Translational Perspective](#)Jixuan Wang; Bin Deng  ; Tianshi Gao; Jiang Wang; Guosheng Yi   ; Ruofan Wang

Chaos 30, 073130 (2020)

<https://doi.org/10.1063/5.0007006>View  
OnlineExport  
Citation

CrossMark



# Chaos

Special Topic: Nonautonomous Dynamics  
in the Climate Sciences

**Submit Today**



# Frequency-dependent response in cortical network with periodic electrical stimulation

Cite as: Chaos 30, 073130 (2020); doi: 10.1063/5.0007006

Submitted: 9 March 2020 · Accepted: 24 June 2020 ·

Published Online: 20 July 2020



View Online



Export Citation



CrossMark

Jixuan Wang,<sup>1</sup> Bin Deng,<sup>1</sup> Tianshi Gao,<sup>1</sup> Jiang Wang,<sup>1</sup> Guosheng Yi,<sup>1,a)</sup> and Ruofan Wang<sup>2</sup>

## AFFILIATIONS

<sup>1</sup>School of Electrical and Information Engineering, Tianjin University, 300072 Tianjin, China

<sup>2</sup>School of Information Technology Engineering, Tianjin University of Technology and Education, 300222 Tianjin, China

**Note:** This paper is part of the Focus Issue on Dynamical Disease: A Translational Perspective.

**a) Author to whom correspondence should be addressed:** guoshengyi@tju.edu.cn

## ABSTRACT

Electrical stimulation can shape oscillations in brain activity. However, the mechanism of how periodic electrical stimulation modulates brain oscillations by time-delayed neural networks is poorly understood at present. To address this question, we investigate the effects of periodic stimulations on the oscillations generated via a time-delayed neural network. We specifically study the effect of unipolar and asymmetric bidirectional pulse stimulations by altering amplitude and frequency in a systematic manner. Our findings suggest that electrical stimulations play a central role in altering oscillations in the time-delayed neural network and that these alterations are strongly dependent on the stimulus frequency. We observe that the time-delayed neural network responds differently as the stimulation frequency is altered, as manifested by changes in resonance, entrainment, non-linear oscillation, or oscillation suppression. The results also indicate that the network presents similar response activities with increasing stimulus frequency under different excitation–inhibition ratios. Collectively, our findings pave the way for exploring the potential mechanism underlying the frequency-dependent modulation of network activity via electrical stimulations and provide new insights into possible electrical stimulation therapies to the neurological and psychological disorders in clinical practice.

Published under license by AIP Publishing. <https://doi.org/10.1063/5.0007006>

Oscillations in brain activity can be controlled by external stimulations. Understanding the mechanism underlying how electrical stimulations modulate brain oscillations may help us to develop new therapies for neurological diseases. In this paper, we demonstrate how the oscillations generated by a time-delayed neural network respond to periodic stimulations of varying stimulation frequency and amplitude. During low-frequency stimulations, the network response is locked to the stimulation frequency and is defined as entrainment. When the stimulation frequency is close to the intrinsic frequency or multiples of its integer, the network resonates, thus enhancing the amplitude of the intrinsic oscillation. For high-frequency stimulation, the network response manifests as abnormal oscillations or oscillation suppression. The results show that the effect of periodic stimulation on the behaviors generated by the time-delayed neural network depends strongly on stimulus frequency. Collectively, the results provide new insights into the potential mechanism underlying the modulation of electrical stimulation. The frequency-dependent response modulation mechanism contributes to possible electrical stimulation therapies for neurological disorders in clinical practice.

## I. INTRODUCTION

Oscillations are ubiquitous in nearly all parts of the brain and at all scales of the locality.<sup>1,2</sup> These oscillations are shaped by neuronal interactions and represent a typical manifestation of intrinsic activity.<sup>3,4</sup> Alpha rhythms in spontaneous oscillations are pivotal to a diverse array of neurological functions, including memory, cognition, and learning.<sup>5,6</sup> Electrical stimulations are engaged in modulating alpha rhythms,<sup>7,8</sup> which suggest that the modulation of brain oscillations via electrical stimulation is a promising clinical option.<sup>9</sup> Many researchers have become increasingly intrigued by the effect that electrical stimulation has on brain oscillations, where they focused on specific stimulus frequencies and amplitudes.<sup>10–13</sup> The mechanism underlying the effects of periodic stimulations on cortical oscillations has yet to be elucidated. In addition, a number of experimental works have paid attention to different stimulation frequencies on brain oscillations,<sup>10,11,13</sup> and it remains imperfect to model the relationship between the responses and stimulations theoretically.

In the present study, we investigate the way in which the time-delayed neural network responds to electrical stimulations,

using the findings of previous studies as a starting point. Previous research has demonstrated that the brain function can be improved by external intervention.<sup>14</sup> Synchronization of the brain to an external stimulus is known as “entrainment.” “Resonance” is a special form of entrainment (the ratio of the stimulation frequency to the intrinsic frequency is  $n:m$ ). Entrainment is accompanied by sensory changes.<sup>15</sup> Previous research, involving the rat model, demonstrated that low-intensity electrical stimulation and external stimulus could entrain oscillations in the rat cortex.<sup>10,11</sup> Within a very narrow frequency band of anode square stimulation, the visual cortex has the potential to generate entrainment to the stimulus.<sup>12</sup> Furthermore, periodic patterns have also been detected following rhythmic stimulation, although the specific manifestation of such patterns have yet to be reported.<sup>16</sup> From an experimental point of view, the phenomenon of synchronization, including resonance and entrainment, has been described in detail within a range of experimental stimulation frequencies. For example, Herrmann recorded human electroencephalogram (EEG) data under flickering light at varying frequencies and detected a resonance response in the beta band.<sup>13</sup> However, these experiments were limited to a certain stimulation frequency or a narrow band of stimulation frequencies. Consequently, little is known about how periodic stimulations systematically shape cortical oscillations. In addition to the stimulation frequency, the cortical network responded with resonance when simulated by a sine wave.<sup>8</sup> Different waveforms may also result in different responses at the same frequency. For example, Brunel *et al.* reported that the rhythm of the oscillations produced was associated with the excitation–inhibition ratio; the higher the ratio, the slower the oscillation.<sup>17</sup> Consequently, future research should study a network’s responses to different intrinsic frequencies from the aspect of the excitation–inhibition ratio.

From the viewpoint of the non-linear dynamics theory, the cortical network can be considered a self-sustained oscillator in which periodic electrical stimulations can be treated as an external force. Many periodically forced oscillatory systems exhibit  $n:m$  ( $n$  represents the number of oscillation cycles while  $m$  represents the number of stimulus cycles) phase locking as well as chaotic dynamics depending on the stimulation parameters.<sup>18</sup> Each entrainment corresponds to one phase-locking value. The phase-locking region formed by the parameters, which is similar to the shape of a tongue, is referred to “Arnold tongue”;<sup>19</sup> this parameter is an essential tool for measuring the type of synchronization under external force. However, the exact manner by which the periodic electrical stimulations can exert influence on synchronous activities has yet to be investigated and a number of focus issues remain unresolved. For example, we do not know what types of phase-locking patterns appear under periodic stimulations, nor do we know whether periodic stimulations with or without noise generate diverse phase-locking patterns. In the present study, we attempt to address these important questions.

Synchronous processes in biological oscillators have been characterized at the theoretical level.<sup>20,21</sup> In this article, we report a cortical network (the oscillator) that makes use of the mean field potential to perform its computations. The advantage of the mean field theory is that the error, which is caused by noise and other factors, can be corrected.<sup>22</sup> However, the influence of noise on synchronization is not negligible. Noise can significantly change the phase-locking

patterns.<sup>23</sup> In the absence of noise, narrow synchronization could only be observed.<sup>24</sup> With an increase in noise intensity, the phase lock will be gradually enhanced.<sup>25</sup> With the addition of dichotomic noise, the phase synchronization will be enhanced.<sup>26</sup> The model utilized in the present study features noise; thus, we make specific efforts to study the effect of noise on synchronization in response to periodic stimulations.

In this paper, we investigate the effect of periodic electrical stimulus on a cortical network. This network generates entrainment, resonance, non-linear oscillation, or oscillation suppression in response to unipolar stimulations and asymmetric bidirectional pulse stimulations. In particular, we focus on the specific effects induced by different stimulus frequencies. Simulations are created in a time delay cortical network, which is able to generate  $\sim 10$  Hz of spontaneous alpha oscillation. Previous studies have exclusively focused on a specific stimulation frequency or a narrow frequency band exclusively. Thus far, stimulations of a specific frequency have been successfully used to treat neurological disorders, although the mechanisms underlying the effects of such periodic stimulations have yet to be fully elucidated. Understanding how periodic stimulations modulate brain oscillations may be the key to developing novel treatments and optimizing existing techniques. We subject the cortical network to a wide range of stimulation frequencies and intensities, and reveal the specific response rules of the network under periodic stimulations. Finally, we generate the cortical network with variable dominant frequencies by changing the excitation–inhibition ratios, subjected the network to electrical stimulations, and then observe the results in terms of the response frequency. The models and results have helped to define a previously unrecognized delayed neural network responding mechanism under electrical stimulations.

## II. MODEL AND METHODS

To simulate the oscillation activity, we choose a modified model proposed by Hutt *et al.*,<sup>27</sup> which describes a delayed neural network. Cortical network model in the presence of electrical stimulation is introduced in this paper. The network initially consists of two populations of excitatory and inhibitory neurons whose membrane potential  $u_n$  obeys the following equation:

$$\alpha^{-1} \frac{d}{dt} u_n(t) = -u_n(t) + N^{-1} \sum_{m=1}^N w_{nm} X_m(t - \tau) + I_n(t) + I_{stim}(t), \quad (1)$$

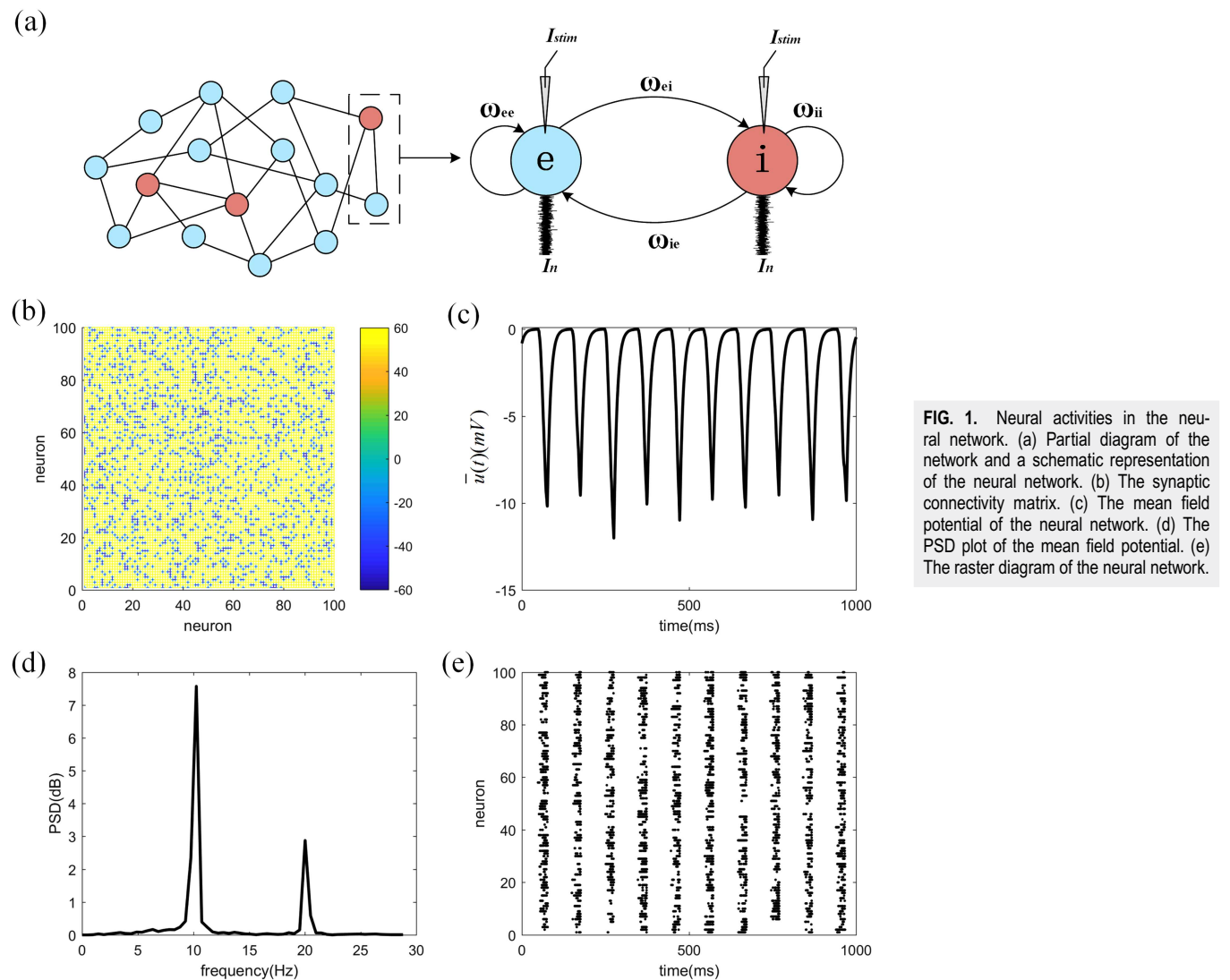
where  $\alpha$  represents the mean membrane time constant while  $N$  represents the size of the neuronal population. Marcus and Westervelt<sup>28</sup> were the first to introduce the delayed neural network model. Time delay  $\tau$  is adopted in our model, which is inevitable on account of the limited information transmission speed between synapses.  $u_n$  represents the resting potential that is subjected to inputs from the presynaptic spike trains  $X_m(t)$  and the stochastic noises  $I_n(t)$  in the case of no external stimulations  $I_{stim}(t)$ . The presynaptic spiking activity obeys the non-homogenous Poisson processes,

$$X_n(t) \rightarrow \text{Poisson}(f(u_n)), \quad (2)$$

where  $f(u_n)$  represents the firing rate function, which is defined by  $f(u_n) = [1 + \exp(-\beta(u_n - h))]^{-1}$ .  $\beta$  and  $h$  refer to the gain and

threshold, respectively.  $f(u_n)$  is approximately equivalent to the Heaviside step function with the definition of  $f = 1$  when  $u_n > h$  and 0 otherwise. Due to the fact that the time scale of dendritic currents is much larger than the firing rate of the population,<sup>29</sup> we consider that  $f(u_n) \approx X_n$ .  $X_n(t) = \sum_{\{t_j\}} \delta_n(t - t_j)$  represents the spike train of the  $n$ th neurons in the population of  $e$  or  $i$ . In addition,  $w_{nm}$  represents the two-dimensional matrix of synaptic strength, thus representing the synaptic strength among the neurons in the network. Considering that the aim is to evaluate the synchronization of oscillations, we choose sparse and random network connections in order to avoid localized oscillation activity.<sup>30</sup> For the sake of simplicity, the synaptic connectivity of our network follows a random distribution: the connection matrix described in Fig. 1(b) is defined by

$$w_{nm} = \mu_n + s_n \xi_{nm}, \quad (3)$$



where  $\{\mu_e, \mu_i\} \subset \mu_n$ ,  $\{s_e, s_i\} \subset s_n$ .  $\mu_i$  and  $\mu_e$  represent the mean synaptic strength of the inhibitory and excitatory neurons.  $s_i$  and  $s_e$  represent the variance of the synaptic strength.  $\xi_i$  is the zero-mean maintaining with  $\xi_j$  and satisfies  $\langle \xi_i(t)\xi_j(t') \rangle = \delta_{ij}\delta(t - t')$ . An illustration of the random connections between the neurons is demonstrated in the left part of Fig. 1(a). The excitatory neurons provide excitatory connections to and receive inhibitory connections from the inhibitory neurons. The inhibitory neurons also have self-inhibitory connections to themselves [shown on the right-hand-side of Fig. 1(a)].

We take advantage of the afferent stochastic noise to mimic inputs from other synaptic neurons, which is given by the independent Gaussian white noise processes,

$$I_n(t) = \sqrt{2D}\xi_i(t). \quad (4)$$

**FIG. 1.** Neural activities in the neural network. (a) Partial diagram of the network and a schematic representation of the neural network. (b) The synaptic connectivity matrix. (c) The mean field potential of the neural network. (d) The PSD plot of the mean field potential. (e) The raster diagram of the neural network.

In the absence of stimulation, recurrent interactions between  $e$  and  $i$  populations generate spontaneously intrinsic synchronous oscillation activity. The mean field potential, the power spectral density (PSD), and the raster diagrams are given in Figs. 1(c)–1(e). Collectively, these diagrams indicate that the network presents spontaneous synchronous activity at the intrinsic frequency of  $\sim 10$  Hz without stimulation.

To emphasize the effect of the electrical stimulations on the brain oscillation activity, we consider two periodic waveforms: single anodic stimulations and asymmetric biphasic pulse stimulations, which contain a time interval between the cathodic and anodic phases. The stimulation with different shapes is applied to the network at the whole stimulation process.

First, we use the single anodic waveform as shown in Fig. 2(a), which is described by Eq. (5).  $t_n = 1000 n/F$  ms,  $n = 0, 1, 2, \dots$ , represent the interval times for the onset of pulses.  $F$  represents the stimulation frequency,  $a$  represents the anodic stimulation intensity, and  $PW$  represents the pulse width ( $PW$ ),

$$I_{stim}(t) = \begin{cases} a, & \text{if } t_n \leq t < t_n + PW, \\ 0, & \text{otherwise,} \end{cases} \quad t \in [t_n, t_{n+1}). \quad (5)$$

In addition to the single anodic waveform, we also take advantage of the charge-balanced biphasic pulses. According to clinical trials, the administration of charge-balanced biphasic pulse inputs has zero net charge when injected into a neuron and thus avoids neuronal damage. The biphasic pulses are advantageous when compared with single anode or single cathode.<sup>31</sup> The equation for the charge-balanced biphasic pulses is

$$I_{stim}(t) = \begin{cases} a, & \text{if } t_n \leq t < t_n + PW, \\ 0, & \text{if } t_n + PW \leq t < t_n + PW + GW, \\ b, & \text{if } t_n + PW + GW \leq t < t_n \\ & + a * PW / b + GW, \\ 0, & \text{otherwise,} \end{cases} \quad t \in [t_n, t_{n+1}), \quad (6)$$

where  $b$  represents the cathodic stimulation intensity while  $GW$  represents the interphase time gap width between the biphasic pulses. The charge-balanced biphasic pulses exhibit a different pulse width ( $PW$ ). The  $PW$  of the anodic pulse is fixed at 1 ms while  $b$  is set to 1 mA. Based on these settings,  $a$  is limited to a maximum value of  $1000/F-2$  mA. Figure 2(b) shows an asymmetric biphasic pulse along with parameter settings.

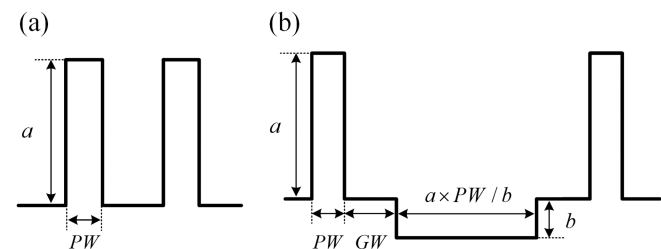


**FIG. 2.** The diagrams of the stimulation waveforms. (a) Single anode pulse stimulation. (b) Charge-balanced biphasic pulse stimulation.

Next, we simulate the results of the same stimulations described above using different excitation–inhibition ratios in order to gain a better understanding of the stimulations. The excitation–inhibition ratio is defined as

$$r = N_i/N. \quad (7)$$

To testify the effect of the stimulations on the dynamics of the oscillation activity, we adopt an expressing of the network dynamics from the point of the ensemble average. To this end, the mean field representation of the network is adopted to simplify the network with the form as follows:

$$\bar{u}(t) = \frac{1}{N} \sum_i u_i(t)/N. \quad (8)$$

In this study, we use the dominant frequency of alpha rhythms, a neural marker of cognitive competence, to observe the variation of brain oscillations.<sup>6,32</sup> The stimulated dominant frequency could be detected from the PSD of the mean field membrane signals. By calculating the PSD, the x-coordinate corresponded to the peak value of the PSD can be used to describe the dominant frequency. PSD analysis is performed using the basic periodogram function in MATLAB R2017a software, which returns two-sided periodogram estimates at the frequencies specified in the vector. All simulations are acquired from at least 100 independent runs to guarantee statistical accuracy. The direct current component of the PSD is removed by subtracting the mean value of  $\bar{u}(t)$  from  $\bar{u}(t)$ .

In addition, in the calculation of the PSD, the first 1000 ms of the simulation results are eliminated to exclude the effects of the transition process. The settings of all parameters used in this study are given in Table I. The simulations are implemented in MATLAB R2017a software using the forward Euler method with a time step of 1 ms for a duration of 4000 ms.

**TABLE I.** Parameter settings.

| Symbol   | Definition                              | Value         |
|----------|---|---------------|
| $\mu e$  | Mean synaptic strength of $e$           | 60            |
| $\mu i$  | Mean synaptic strength of $i$           | -60           |
| $se$     | Mean synaptic standard deviation of $e$ | 0.01          |
| $si$     | Mean synaptic standard deviation of $i$ | 0.01          |
| $\beta$  | Response function gain                  | 2500 mV       |
| $h$      | Firing threshold                        | 0 mV          |
| $D$      | Noise intensity                         | 0.01          |
| $N$      | Number of neurons                       | 100           |
| $\tau$   | Time delay                              | 25 ms         |
| $\alpha$ | Membrane time constant                  | 100 Hz        |
| $N_i$    | The number of inhibitory neurons        | 200           |
| $N_e$    | The number of excitatory neurons        | 800           |
| $R$      | The excitation–inhibition ratio         | 0–1           |
| $a$      | Anodic stimulation intensity            | 0–1000/F-2 mA |
| $b$      | Cathodic stimulation intensity          | 1 mA          |
| $F$      | Stimulation frequency                   | 0–200 Hz      |
| $PW$     | Pulse width                             | 1 ms          |
| $GW$     | Gap width                               | 1 ms          |
| $dt$     | Integrate time step                     | 1 ms          |

### III. RESULTS

#### A. Impact of single anodic stimulation

The effects of the stimulation frequencies created by a single anode on the delayed neural network are quantified, and three typical network responses are recorded. These observations imply that different stimulation frequencies activate different response mechanisms. Membrane potential shows spontaneous subthreshold oscillations without any external stimulation, as shown in Fig. 3(a). Spontaneous synchronization is maintained at the intrinsic frequency ( $\omega_f$ ) of  $\sim 10$  Hz. The network responds as resonance when  $F$  reaches 10 Hz. As illustrated in Fig. 3(b), the amplitude of the dominant frequency ( $\omega_{\max}$ ) in PSD increases obviously while the dominant frequency barely changes. As shown in Fig. 3(c),  $\omega_{\max}$  is locked to  $F$  and the dynamics of the network shows entrainment. As the stimulation frequency increases,  $\omega_{\max}$  shows a significant difference compared with the initial intrinsic frequency. The essence of the change in intrinsic frequency is the alteration in the duration of the inter-spike interval duration, which reflects a new encode information. In other words, the initial intrinsic frequency is reshaped and the network induces non-linear oscillation when  $F$  approaches 200 Hz, as revealed in Fig. 3(d).

The simulation results indicate that different stimulation frequencies could generate different response activities, which are determined by  $\omega_f$  and  $F$ . Without stimulation, the network generates  $\omega_f$  reflecting the basic characteristics of the network. In the case of stimulus, the network exhibits three responses: (1) when  $F$  is an integer multiple to  $\omega_f$ , such a situation is termed as resonance and the dominant frequency is approximate to the intrinsic frequency ( $\omega_{\max} \approx \omega_f \approx F/n$ ); (2) when  $F$  is proportional to  $\omega_f$ , we consider it as entrainment ( $\omega_{\max} \approx \omega_f \approx F * m/n$ ); (3) when the stimulation alters the network's intrinsic frequency, the action is called as non-linear oscillation. To have a better acknowledgment of the relationship between  $F$  and  $\omega_{\max}$ , we combine the PSD for various stimulation frequencies. Figure 4(a) shows PSD as a function of the two frequencies,  $F$  and  $\omega_f$ . It is helpful for distinguishing synchronous states. The guide for interpreting PSD is displayed in Fig. 4(b). Continuous lines with an upward slope depict different synchronized response types. The synchronous response types can, therefore, be distinguished by analyzing their relative slopes. Specifically, when the fundamental frequency is arranged diagonally, the harmonic peaks are distributed in the upper left half of the diagonal while the subharmonic peaks are distributed in the lower right half of the diagonal. Furthermore, we observe that  $\omega_{\max}$  is an

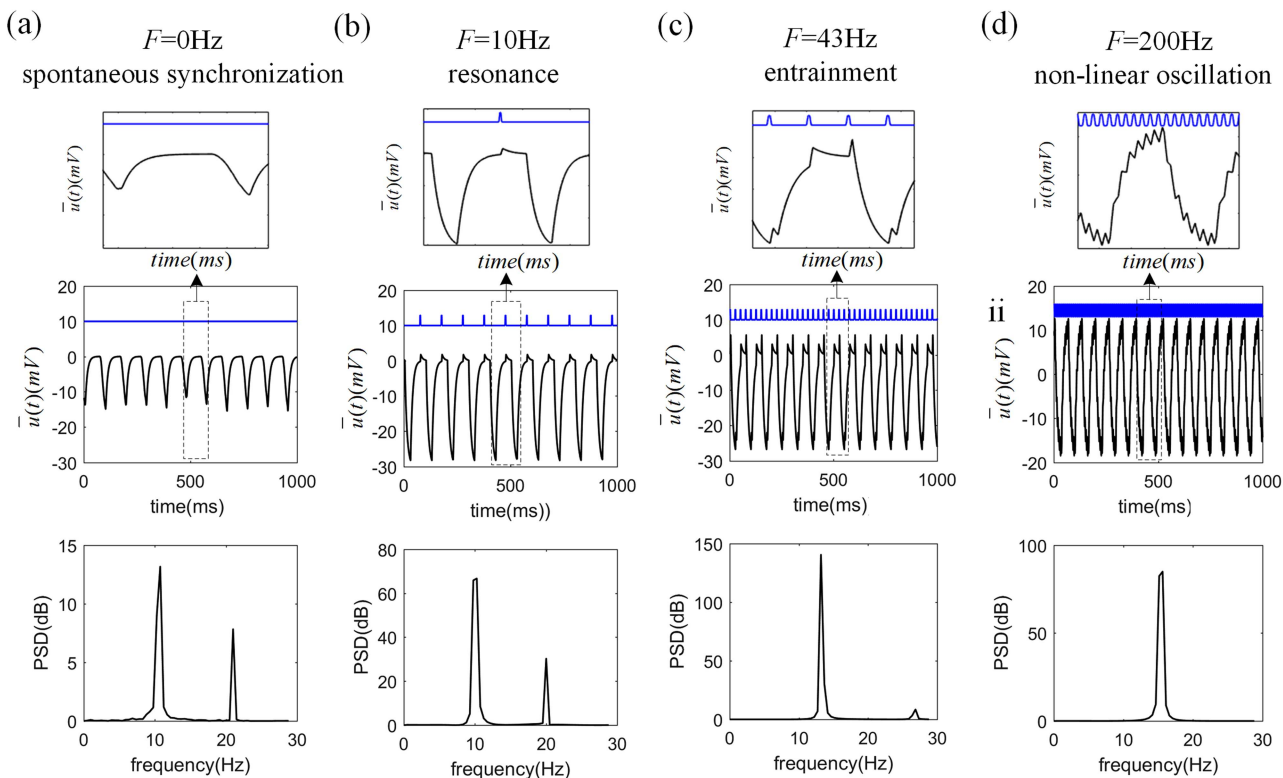


**FIG. 3.** The dynamics of the network when stimulated by a single anode. The top panel shows boxes of enlarged detail showing mean field potentials and stimulations. The middle panel shows mean field potential under different stimulus frequencies. The bottom panel shows the PSD of the mean field potential. For clarity, the stimulus amplitude showed in (b)–(d) is narrowed to the third of the actual one ( $a = 10$  mA).

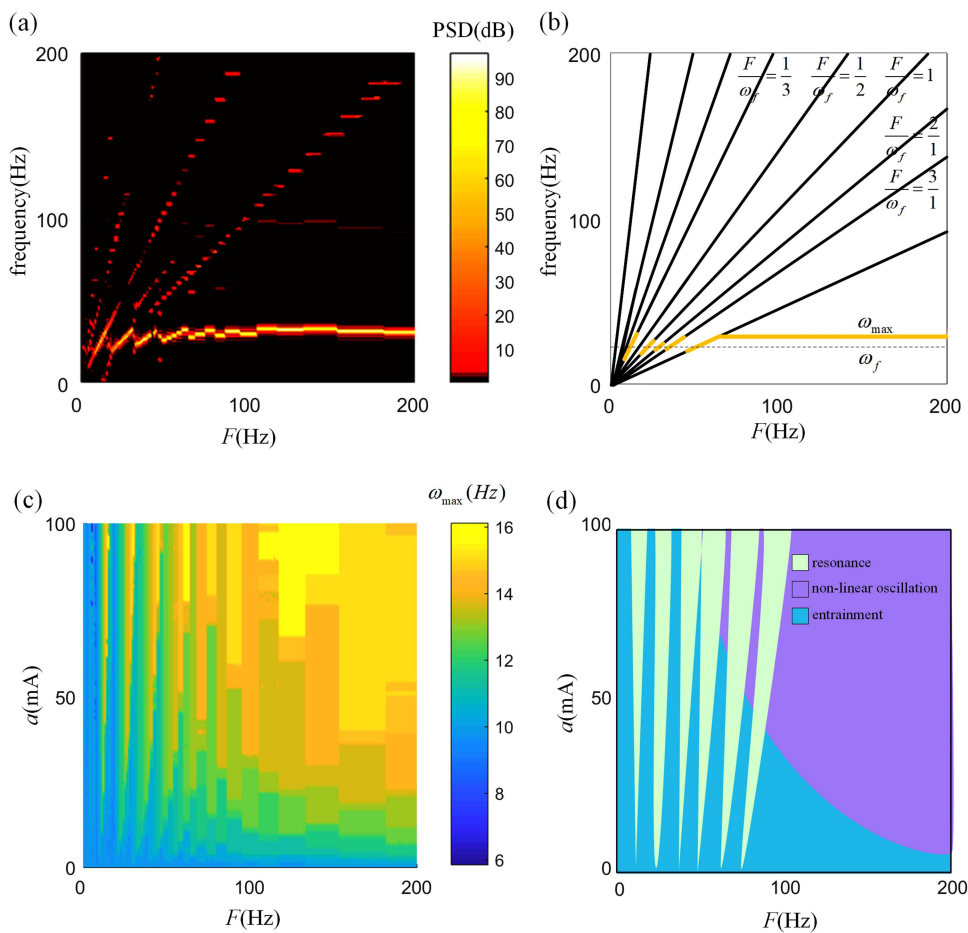


**FIG. 4.** (a) Color map of PSD for different stimulation frequencies with a fixed stimulation intensity ( $a = 3 \text{ mA}$ ). The diagonal refers to the fundamental frequency. The harmonics and subharmonics of the stimulation frequency are aligned above and below the diagonal, respectively. (b) An abridged general view of (a) in which the shift of the dominant frequency is highlighted in solid yellow. Harmonics ( $F/\omega_f < 1$ ) and subharmonics ( $F/\omega_f > 1$ ) present continuous distribution. (c) Color map of dominant frequency in PSD following unfolding of the stimulation intensities. Resonance and entrainment are aligned vertically and alternatively at lower stimulus frequencies ( $0 < F < 100 \text{ Hz}$ ). Non-linear oscillation occurs at higher frequencies ( $F > 100 \text{ Hz}$ ). (d) The diagrammatic drawing of (c) in which the resonance, entrainment, and non-linear oscillation are labeled.

integer multiple to  $F$  when harmonics are produced, demonstrating the existence of a strong resonance effect. Furthermore, entrainment is accompanied with a subharmonic component,  $\omega_f$ , of the network offsets to  $\omega_{\max}$ , which changes the intrinsic frequency. At the point of non-linear oscillation, the network acts as fast oscillation. It is evident from Fig. 4(b) that  $\omega_f$  maintains a constant with slight fluctuation in which the stimulus has little effect.

Due to the limitation of stimulation amplitude in Fig. 4(a), we detect the systematic alteration of  $\omega_{\max}$  for varied  $a$  and  $F$ .  $a$  changes from 0 to 100 mA with an increment of 0.5 mA, while  $F$  ranges from 0 to 200 Hz with an increment of 1 Hz. By changing  $a$  and  $F$ , it allows us to control the stimulation conditions that result in synchronization and to identify the response mechanism. Figure 4(c) shows a color map of  $\omega_{\max}$  depicting the relationship between stimulation amplitude and response type; it is evident that resonance responses are aligned at multiples of  $\omega_f$ . The resonance effect leads to an enhancement in oscillations at about 10 Hz. Entrainment and resonance appear alternately at lower  $F$ . At a sufficient stimulus intensity, resonance and entrainment responses become so strong that they could be readily observed, and each response width becomes larger. Non-linear oscillation is initiated when  $F$  exceeds 60 Hz, which is neither at the intrinsic frequency nor is it in a

synchronous state. Visible response partitions are labeled in Fig. 4(d); in accordance with rhythm variation,  $F$  is able to change the response patterns of the network, including resonance, entrainment, and non-linear oscillation. This leads to a hypothesis that the regularity associated with responses may provide an efficient way to treat diseases. The network response activities are determined mainly by  $F$ , while the increase of  $a$  is shown to amplify the effect. It is evident that the response activities show strong frequency dependence.

Next, we investigate whether the presence or absence of noise could alter the synchronization modes. Synchronous phase-locking patterns are known to be strongly associated with stimulation frequencies. The stimulation intensities can promote or impede synchronous activities. Phase-locking patterns triggered by different stimulation frequencies follow a typical Arnold tongue rule. Figures 5(a) and 5(b) show Devil's staircases with or without noise, which intuitively exhibit phase-locking patterns and synchronous widths. The width of the flats shown in Figs. 5(a) and 5(b) corresponds to the width of the Arnold tongue under the corresponding amplitude ( $a = 3 \text{ mA}$ ). Furthermore, the width of the flats is constant when the ratio of  $F$  to  $\omega_{\max}$  is around a rational value:  $F/\omega_{\max} = m/n$ , in which  $m$  and  $n$  are integers. Each flat remains constant

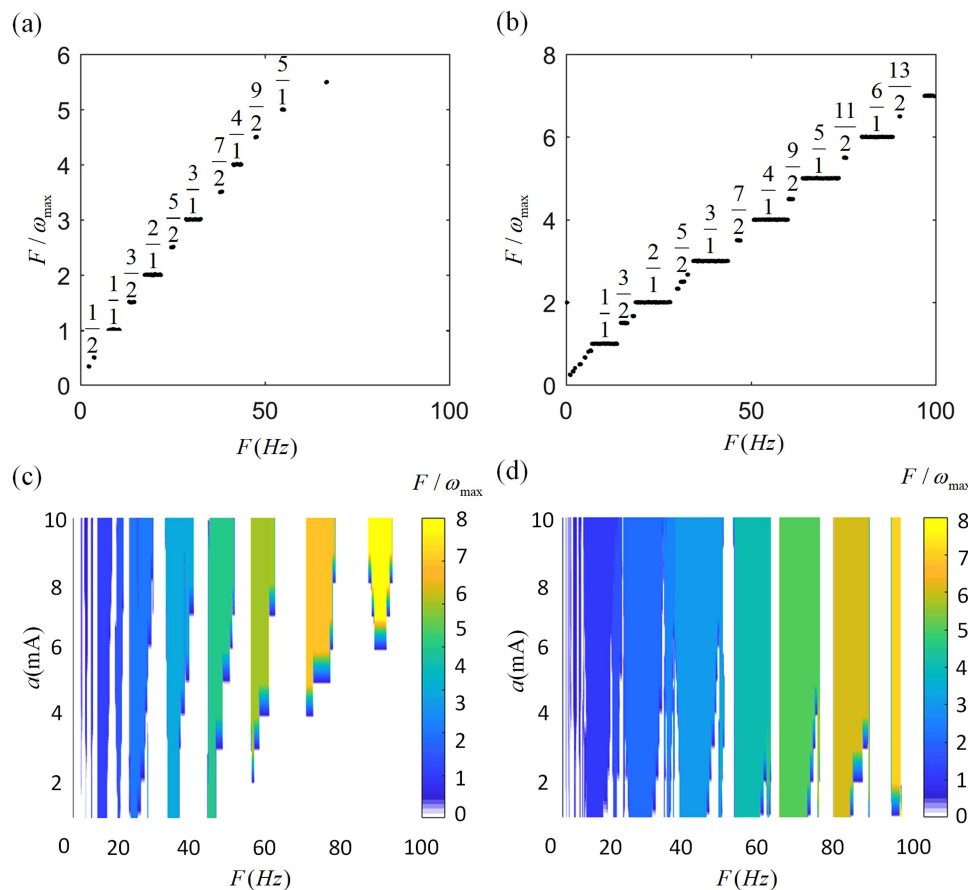


**FIG. 5.** Devil's staircases and Arnold tongues of the network in response to single anode stimulations with or without noise. Devil's staircases are useful that they allow us to clearly observe a range of stimulation frequencies in a synchronous state. The flats indicate typical harmonics and subharmonics. For the sake of clarity, we delete the non-obvious phase-locking value between the flats. Arnold tongues represent regions in which various phase-locking states exist. (a) Devil's staircases with noise ( $a = 3$  mA). The order of transitions between flats is displayed. (b) Devil's staircases without noise ( $a = 3$  mA). In the absence of noise, some new phase-locking values appear and the width of each phase lock becomes significantly larger. (c) Arnold tongue diagram with noise showing a clear arrangement of tongues. As  $a$  increases, the phase-locking regions expand although there is a reduction in the number of phase-locking types. (d) Arnold tongue diagram without noise. Compared to (c), the tongues are notably wider. In the lower part of a, many narrow tongues are evident (i.e., 1/4 and 3/4).

for a period of  $F$ , indicating that  $\omega_{\max}$  is locked to  $F$  for a finite range of increasing  $F$ . In the absence of noise, a greater number of wider flats are generated. Some subharmonic values appear in the vicinity of 1/1 Devil's staircases, including 1/4, 1/5, and 2/3. Figure 5(c) shows the Arnold tongue accompanied by noise; in this figure, there are fewer phase-locking types with a narrower synchronization width when compared with the Arnold tongue without noise that is shown in Fig. 5(d). The phase-locking patterns in the Arnold tongue diagram are highly variable at the same frequency. Notably, differing amplitudes at the same stimulation frequencies appear to generate different phase-locking patterns. The widths of the Arnold tongues decrease (i.e., 3/2, 5/2, and 7/2) as  $a$  increased. Overlapping the phase-locking regions (i.e., 1/1, 2/1, and 3/1) makes some tongues disappear (i.e., 3/2, 5/2, and 7/2). As  $F$  increases, the Arnold tongues for the van der Pol oscillator become so narrow that they are difficult to observe. Larger period  $m$  of  $m/n$  phase locking generates a narrower tongue. In contrast, some tongues (i.e., 4/1 and 5/1) are still easy to observe and span a wide range of stimulation frequencies irrespective of whether noise is present or not. More simplistically, it is evident that the model is more idealized in the absence of noise; as a result, a larger phase-locking region appears. We report a cortical network making use of the average field potential to perform its computations. The advantage of the mean field theory is that the

error caused by noise and other factors could be corrected. Therefore, the tongues are also relatively evident when there is an increase in the period  $m$  of  $m/n$  phase locking.

## B. Role of asymmetric bidirectional pulse stimulation

Considering the influence of different stimulus waveforms, we have simulated single cathodic stimulations, symmetric bidirectional pulse stimulations ( $a = b$ ), and asymmetric bidirectional pulse stimulations ( $b > a$ ). The results (data not shown) confirm that oscillations are suppressed by intracellular stimulations. The hyperpolarization observed in our present data is consistent with Yi and Grill who proved that inhibitory inputs could abolish excitability in the soma by extracellular stimulations.<sup>10</sup> We adopt intracellular stimulations in the present study instead of extracellular stimulations. More importantly, our results indicate that the stronger the cathodic stimulation intensity becomes, the more suppressed the oscillations would become. Considering that the injection of charge arising from unipolar stimulation might impair cerebral function,<sup>33</sup> we apply asymmetric bidirectional pulse stimulations ( $a > b$ ) to ensure that neuronal firing activities maintain normal. We also estimate energy consumption (Fig. 6) and found that the energy consumption of the asymmetric bidirectional pulse stimulations is lower

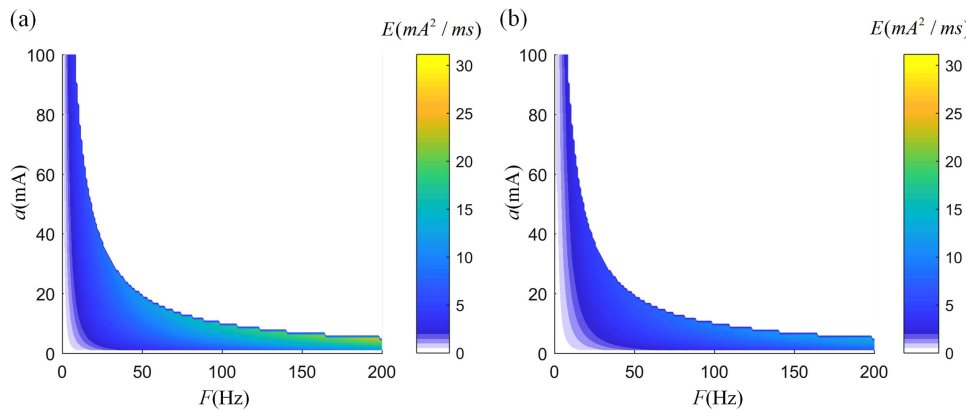
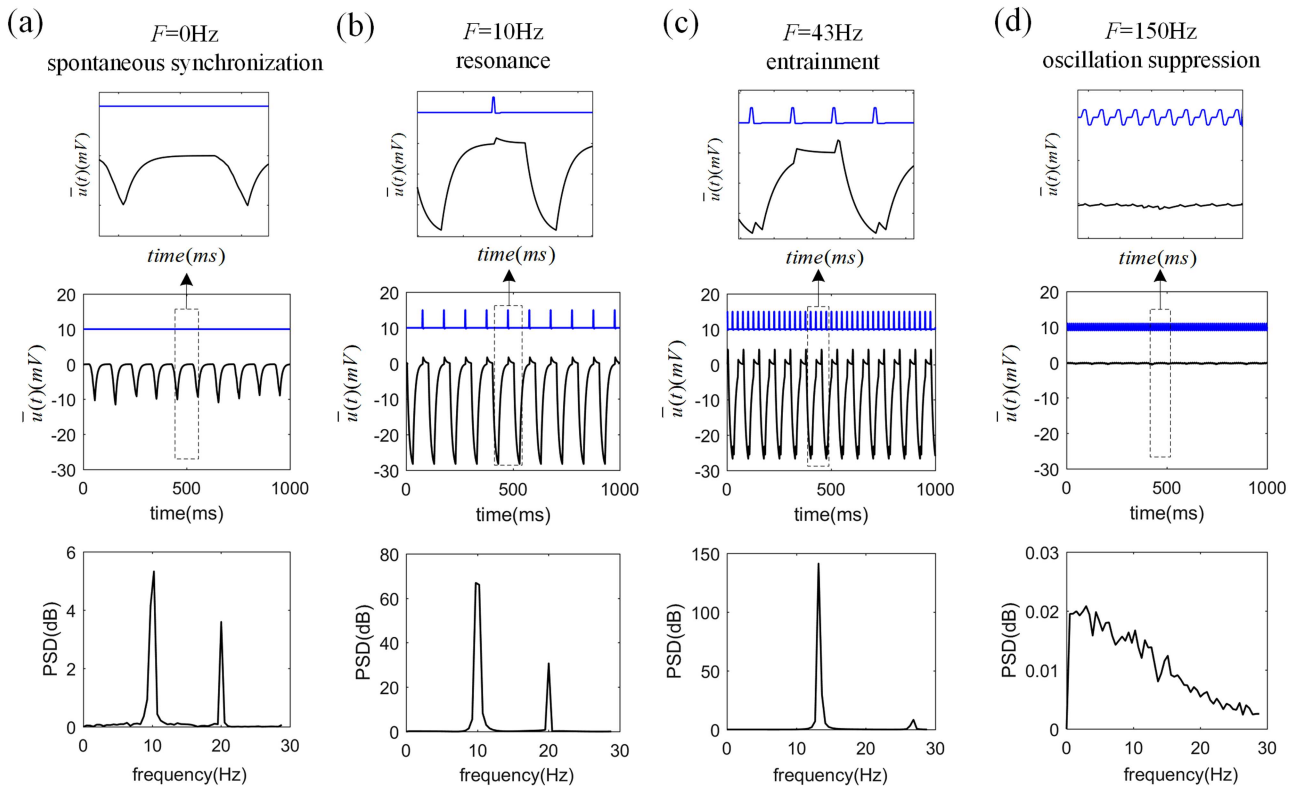


**FIG. 6.** Energy consumption associated with symmetric (a) and asymmetric (b) bidirectional pulse stimulations. It is clear that asymmetric stimulations consume lower amounts of energy. The color bar represents the total energy consumption associated with the stimulation.

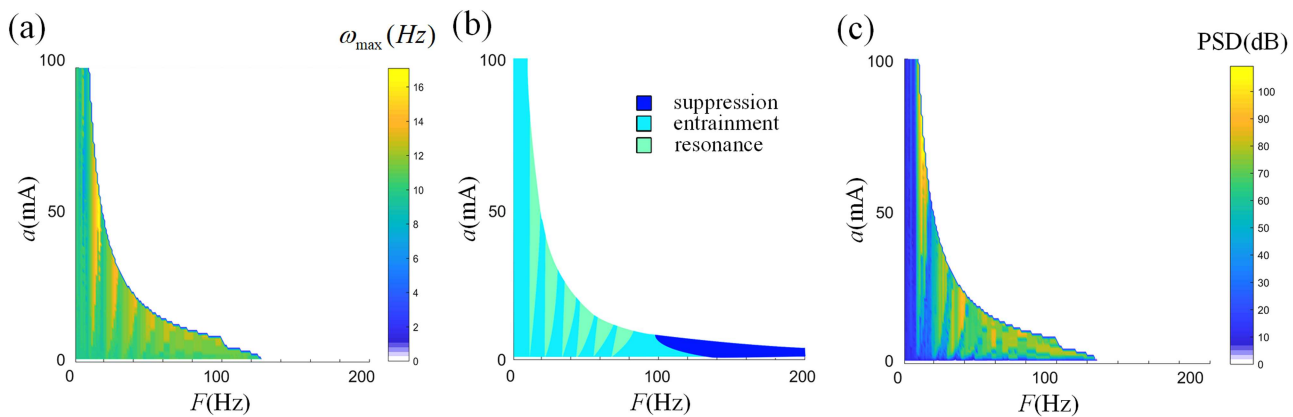
than the symmetric bidirectional pulse stimulations when exposed to equivalent stimulation intensities and frequencies. In conclusion, asymmetric bidirectional pulse stimulations are utilized in this section.

Figure 7 depicts a condition in which the network accepts asymmetric bidirectional pulse stimulations, which shows membrane potential and PSD. The network responses emerge

as resonance and entrainment echoing previous phenomena in Fig. 4(c). As illustrated in Fig. 7(b), the amplitude of  $w_{\max}$  increases significantly and shows strong resonance activity at 10 Hz ( $\omega_{\max} \approx \omega_f \approx F/n$ ). Phase lock  $m/n$  ( $\omega_{\max} \approx \omega_f \approx F * m/n$ ) is observed in Fig. 7(c) and the network responds as entrainment at  $F=43$  Hz. The improvement in upper alpha frequency is known to strengthen the cognitive performance.<sup>34</sup> It is worth noting that the oscillation



**FIG. 7.** The dynamics of the network under asymmetric bidirectional pulse stimulations. The top panel shows an enlarged view of the mean field potentials and stimulations. The middle panel shows the mean field potential at different stimulus frequencies. The bottom panel shows the PSD of the mean field potential. (a)  $a = 0$  mA; (b) and (c)  $a = 5$  mA; (d)  $a = 1$  mA.



**FIG. 8.** (a) Color map of PSD for different stimulation frequencies. (b) The abridged general view for dominant frequency in the PSD of (a). (c) Plot of the power of the dominant frequency in PSD. The color bar in (c) represents the peak corresponding to  $\omega_{\max}$ .

activity of the network is suppressed when  $F$  reaches a higher frequency. Besides,  $\omega_{\max}$  has a slight offset to higher frequency. Oscillations are eliminated for reasons that the enhanced cathodic stimulation aggravates hyperpolarization. Furthermore, the formation conditions of resonance and entrainment are identical to that of single anodic stimulation.

To fully figure out PSD patterns over a range of stimulation parameters, the color graph is unfolded in Fig. 8 across a range of  $a$  and  $F$ . Given the limitation of pulse width and stimulation frequency, the stimulation intensity is limited to a definite scope. As the stimulation intensity ( $a$ ) and stimulation frequency ( $F$ ) change, the network clearly supports three types of response activities, including resonance, entrainment, and oscillation suppression [Fig. 8(b)]. As illustrated in Fig. 8(a), the peaks of the resonance frequencies are arranged at an integral multiple frequency of  $\omega_f$ , which would, therefore, enhance the 10 Hz rhythm. In addition, the intermittent occurrence of entrainment and resonance emerge at the lower frequency band ( $0 < F < 100$  Hz). The PSD displays corresponding variation tendency, which is revealed in Fig. 8(c). Notably, at the higher frequency band ( $100 \text{ Hz} < F < 125$  Hz), the oscillation activity is inhibited when  $a$  increases. Notably, at ultrahigh  $F$  ( $F > 125$  Hz), the response activity of the network is completely suppressed. To avoid oscillation suppression, stimulus intensity and frequency should be carefully selected for related diseases therapy in which the stimulations are introduced. Moreover, unlike single anode stimulations, the asymmetric bidirectional pulses result in oscillation suppression rather than the non-linear oscillation because of the involvement of cathodic stimulation. Intriguingly, the asymmetric bidirectional pulse stimulations not only exhibit resonance and entrainment but also associate with strong frequency dependence like single anode stimulations.

### C. Effect of the excitation-inhibition ratio on the delayed neural network

In order to investigate the potential consequences of the findings obtained in Secs. III A and III B, we next analyze the

correlations between the excitation-inhibition ratio and the network response under stimulations. The only difference between these experiments to those described in Secs. III A and III B is the addition of the excitation-inhibition ratio.

A previous study has confirmed that there is a close relationship between the proportion of inhibitory neurons and the intrinsic frequency. Larger proportion of inhibitory neurons generates higher intrinsic frequency.<sup>17</sup> Differences in the intrinsic frequency may distribute in different bands, such as the theta, alpha, and beta bands. It remains unclear how the delayed neural network with different intrinsic frequencies responds to stimulations. Herein, we attempt to examine the network response under diverse ratios. The response of the network is explored at  $r = 1/5$ . Figure 9 summarizes the network responses for a variety of different ratios. The intrinsic frequency of the network transforms with the variation of the excitation-inhibition ratios. It can be observed that the network shows a similar response to  $r = 1/5$  under different ratios. For lower frequencies, the network responds as resonance at the integer multiples of intrinsic frequency. Entrainment is distributed toward the middle of the resonance. As the frequency increases to higher value, the network changes to produce non-linear oscillations. Notably, the oscillation is impaired when the number of excitatory neurons turns to zero [Fig. 9(k)]. Theoretically, a smaller ratio generates smaller intrinsic frequency; this would generate a greater number of integer multiples for intrinsic frequency across an equivalent scope of stimulations. We find that resonance and entrainment are positively correlated with the integer multiples of the intrinsic frequency. As a consequence, resonance and entrainment are distributed more densely at lower frequencies for small excitation-inhibition ratios. Compared with larger ratios, the region size of the non-linear oscillation is greater than that for lower ratios. Low initial intrinsic frequencies appear to be more likely to form non-linear oscillation. Overall, the network shows resonance, entrainment, and non-linear oscillation, which are in accordance with the aforementioned consequences. To some extent, the network may also yield identical responses across other frequency bands.

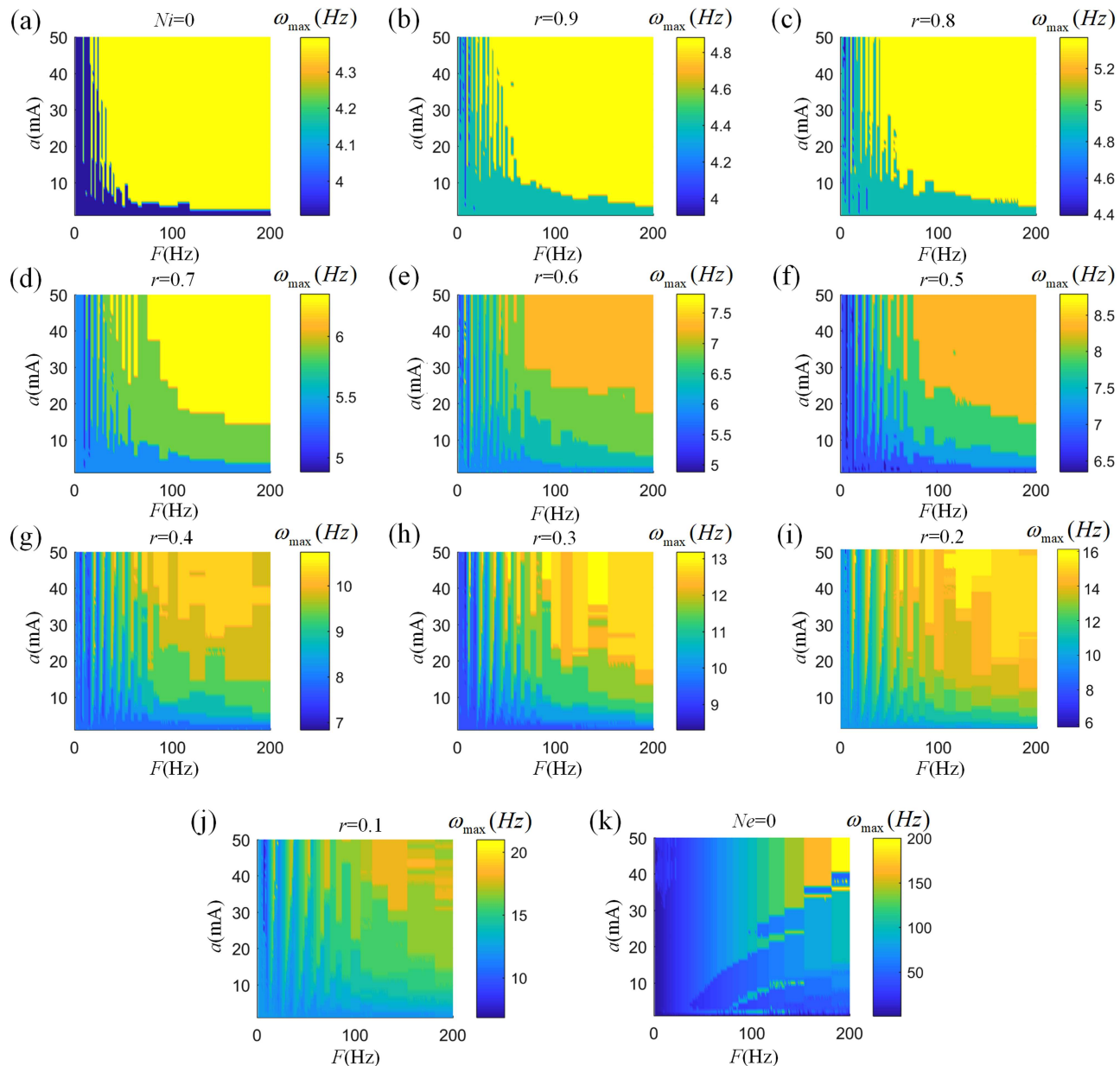


**FIG. 9.** Color maps of dominant frequency in PSD for different ratios when applied by single anodic stimulation. (a) The condition in which there is no inhibitory neurons. (b)–(j) The proportion of inhibitory neurons ranges from 0.9 to 0.1 with an internal of 0.1. Resonance and entrainment at lower frequencies are distributed alternately and are denser due to the small proportion of excitatory neurons. Low initial intrinsic frequencies appear to be more likely to form non-linear oscillation. (k) The condition in which the sum of excitatory neurons is 0.

The next key question is to determine how network oscillations respond to the asymmetric bidirectional pulse stimulations with variable ratios. To solve this question, we conduct a systematic test on disparate ratios under asymmetric bidirectional pulse stimulations. The network responds over a scope of  $r$  ranging from 0 to 1 with an increment of 0.1 and  $F$  ranged from 0 to 200 Hz with an

increment of 1 Hz. As recorded in Fig. 10,  $a$  ranges from 0 to 1000/ $F$ -2 mA and little changes could be detected in terms of the response types, thus suggesting that the simulated activities exhibit similar responses as the ratio changes. There are two general differences evident in these results. First, the intermittent distribution of resonance and entrainment are arranged between 0 and 100 Hz. Furthermore,

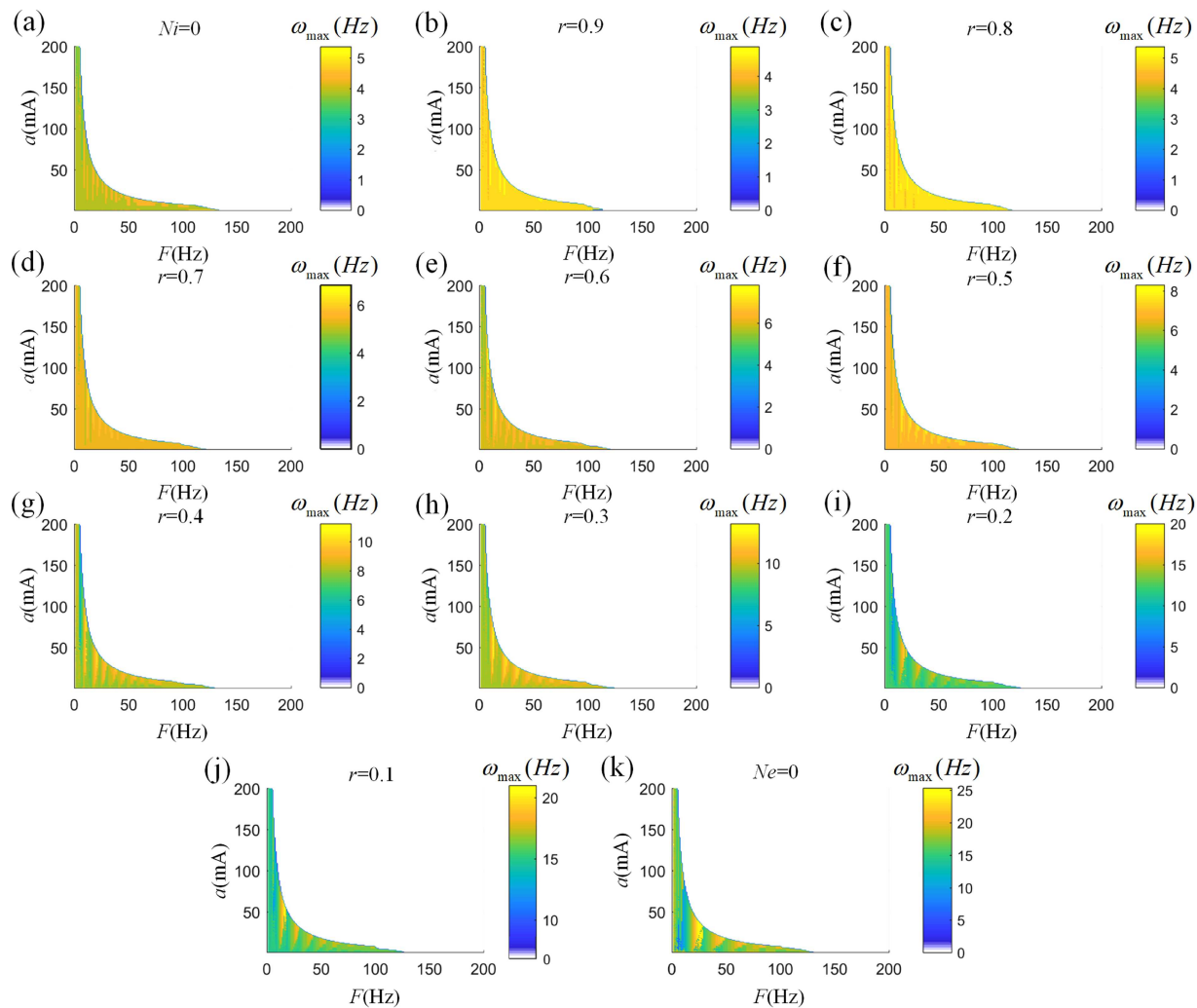


**FIG. 10.** Color maps of dominant frequency in PSD for different ratios via asymmetric indirection pulse stimulation. (a) A condition in which there is no inhibitory neuron. (b)–(j) The proportion of inhibitory neurons ranges from 0.9 to 0.1 with an interval of 0.1. (k) A condition in which there is no excitatory neuron. Resonance and entrainment occur between 0 and 100 Hz. The network responds as oscillation suppression at higher frequencies. The ratios have a negligible effect on the region size of the oscillation suppression.

the distribution rule for lower frequencies is the same as that of a single anodic wave stimulus. Second, the network activity responds as oscillation suppression at higher frequencies. In contrast to single anodic stimulations, the intrinsic frequency has minimal effect on the region size of the oscillation suppression under asymmetric bidirectional pulse stimulations. Cathodic stimulation leads to the hyperpolarization of neurons resulting in the oscillation suppression, and the properties of the inhibitory neurons are crucial to the process of hyperpolarization. Therefore, the change in ratio has little effect on the region size of the oscillation suppression. Suppression could be generated at higher amplitudes, ranging from 100 Hz to 125 Hz. Cathodic stimulation has the ability to generate oscillation suppression within this range, whereas such a phenomenon only

occurs when the intensity is sufficiently large. It is easier to generate oscillation suppression at higher frequencies when stimulated by a cathodic stimulation. Variation in parameter  $r$  has little effect on the network responses. Thus, we propose that the network produces similar responses when experiencing different ratios.

#### D. Theoretical derivation

Next, we aim to investigate the mechanisms underlying how the stimulation frequency may play a role in modulating the rhythms we observe. To do this, we apply mean field theory to describe the network dynamics. We assume that the potential of a neuron can be described by noise fluctuations around the mean field

potential,

$$u_n(t) = \bar{u}(t) + v_m(t), \quad (9)$$

where the mean field potential obeys  $\bar{u}(t) = N^{-1} \sum_{n=1}^N u_n(t)$ .  $v_m(t)$  represents the local fluctuations making the individual neurons fluctuate around the mean field potential while  $v_m(t)$  obeys the Ornstein–Uhlenbeck processes,

$$\frac{d}{dt} v_m = -v_m(t) + I_{stim}(t) - \mu_I. \quad (10)$$

The mean value of  $v_m(t)$  is given by

$$\mu_I = \int_t^{t+\Delta t} I_{stim}(s) ds. \quad (11)$$

We convert Eq. (1) to the integral formula to make the function continuous and integrable. The sum of the function is equivalent to the integral of the probability density function and the original function as  $N \rightarrow \infty$ ,

$$N^{-1} \sum_{m=1}^N w_{mn} X_m(t - \tau) \approx N^{-1} \sum_{m=1}^N w_{mn} f(u_n(t - \tau)). \quad (12)$$

We use Eqs. (9)–(12) and the summation formula to calculate the mean field potential,

$$\begin{aligned} \frac{d}{dt} \bar{u}(t) &= -\bar{u}(t) + \bar{w} \int_{-\infty}^{+\infty} f(\bar{u}(t - \tau) + v_m(t - \tau)) \rho(v) dv + \mu_I \\ &= -\bar{u}(t) + \bar{w} F(\bar{u}(t - \tau)) + \mu_I. \end{aligned} \quad (13)$$

The response function of the neurons is shown as

$$F(\bar{u}) = \int_{v_1}^{v_2} f(\bar{u} + v) \rho(v) dv. \quad (14)$$

First, we consider the response function in the absence of stimulation. We then combine the previous data<sup>27</sup> and find that the

response function obeys the non-linear function,

$$F(\bar{u}) = \frac{\bar{w}}{2} \left( 1 + \operatorname{erf} \left( \frac{\bar{u}(t - \tau)}{\sqrt{2D}} \right) \right). \quad (15)$$

Next, we calculate the response function under single anode stimulation. The mean value of the stimulation is

$$\mu_I(t) = \begin{cases} a, & \text{if } t_n \leq t < t_n + PW, \\ 0, & \text{otherwise,} \end{cases} \quad t \in [t_n, t_{n+1}). \quad (16)$$

Under limitations imposed by  $b, f(u_n)$  is approximately equivalent to the Heaviside step function with the definition of  $f = 1$  when  $u_n > h$  and  $f = 0$  for otherwise. Therefore, the response function could be defined by

$$\begin{aligned} F(\bar{u}) &= a \int_{t_n}^{t_n + PW} \frac{H(\bar{u} + v - h)}{v} dv \\ &= -aH \left( \bar{u} - \frac{1000}{F} - h \right) \left( \ln(-\bar{u}) - \ln \left( \frac{1000}{F} \right) \right) \\ &\quad + aH \left( \bar{u} + \frac{1000}{F} + PW - h \right) \left( \ln(-\bar{u}) - \ln \left( \frac{1000}{F} + PW \right) \right). \end{aligned} \quad (17)$$

Finally, we calculate the asymmetric bidirectional pulse stimulations. We find that a portion of this form of anode stimulation is similar to that of single anode stimulation, while the cathodic stimulation component is very different from anode stimulation. The mean value of the stimulation is defined by

$$\mu_I(t) = \begin{cases} a, & \text{if } t_n \leq t < t_n + PW, \\ 0, & \text{if } t_n + PW \leq t < t_n + PW + GW, \\ b, & \text{if } t_n + PW + GW \leq t < t_n + a * PW/b + GW \\ & + a * PW/b + GW \\ 0, & \text{otherwise,} \end{cases} \quad t \in [t_n, t_{n+1}). \quad (18)$$

The response function is therefore described by

$$\begin{aligned} F(\bar{u}) &= \begin{cases} a \int_{t_n}^{t_n + PW} \frac{H(\bar{u} + v - h)}{v} dv \\ b \int_{t_n + PW + GW}^{t_n + a * PW/b + GW} \frac{H(\bar{u} + v - h)}{v} dv \end{cases} \\ &= \begin{cases} -aH \left( \bar{u} - \frac{1000}{F} - h \right) \left( \ln(-\bar{u}) - \ln \left( \frac{1000}{F} \right) \right) + aH \left( \bar{u} + \frac{1000}{F} + PW - h \right) \left( \ln(-\bar{u}) - \ln \left( \frac{1000}{F} + PW \right) \right) \\ -bH \left( \bar{u} - \frac{1000}{F} + PW + GW - h \right) \left( \ln(-\bar{u}) - \ln \left( \frac{1000}{F} + PW + GW \right) \right) \\ + bH \left( \bar{u} + \frac{1000}{F} + a * PW/b + GW - h \right) \left( \ln(-\bar{u}) - \ln \left( \frac{1000}{F} + a * PW/b + GW \right) \right). \end{cases} \end{aligned} \quad (19)$$

Theoretical data derived from these three cases are depicted in Fig. 11. As shown in Fig. 11(a), the response function is non-linear in the absence of stimulation. Single anode stimulation is able to shape the response function, thus leading to a tendency toward the linearization of response function in which the linear tendency is

more pronounced as the stimulation frequency changes [Fig. 11(b)]. The response function of the resonance stimulation frequency is the steepest while non-linear oscillation shows the smoothest trend. Between these two functions, the network responds as entrainment. The response function generates the entrainment in between of the

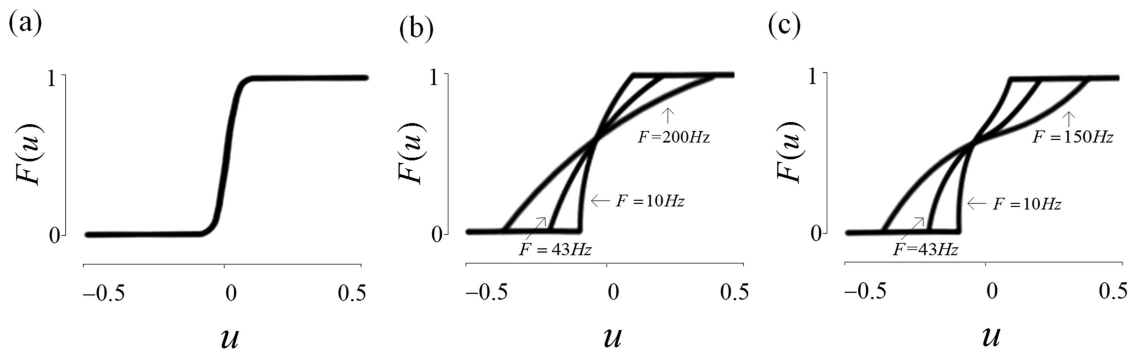


**FIG. 11.** The plots of the response function under different stimulations. (a) The response function in the absence of stimulation. (b) Response function in the presence of single anode stimulation ( $a = 10$  mA). (c) Response function in the case of the asymmetry bidirectional pulse stimulations ( $a = 10$  mA).

two cases above. With regard to asymmetric bidirectional pulse stimulations, the analogous situation is important in terms of the response function. On account of the cathodic stimulation, the response function is different to that shown in Fig. 11(b). Moreover, the response function is slower than anode stimulation when  $u > 0$ . We, therefore, conclude that the linear process is similar to the variation in noise intensity, as reported previously.<sup>27</sup> Frequency-dependent activity is also known to affect the non-linear response function, at least to some extent. Non-linear oscillation and oscillation suppression are the most linearized events. Compared with the situation in the absence of stimulation, the resonance and entrainment caused by stimulation frequency variation both improve the non-linear response function.

#### IV. DISCUSSION AND CONCLUSIONS

At present, the quantitative assessment of the effects of neural stimulation is limited to the stimulation frequency range. In this study, we have made significant stride toward understanding how the neural network responds to electrical stimulations in a powerful frequency-dependent manner. The responses generated by the periodically stimulated, time-delayed neural network include resonance, entrainment, non-linear oscillation, or oscillation suppression. We also investigate phase-locking patterns and Arnold tongues in theoretical analysis with and without noise. In conclusion, the numerous simulation results in this study demonstrate that the parameter determining the network response is the stimulation frequency. In this regime, increased stimulation intensity strengthens the network response, which plays a less important role in altering the network response. The waveforms have a trifling impact on the network response except for the stimulations involving the cathodic stimulus. The network response scarcely swings with the variation of the excitation-inhibition ratio, which further proves that the network processes strong frequency dependence.

A number of experimental studies have investigated the response of an oscillator in response to an external stimulus. However, few theoretical studies have been carried out on the response of a network to periodic stimulus. Our theoretical data concur with the findings of a previous study involving human EEG data.<sup>13</sup> Under 1–100 Hz flickering light, the human EEG presented with

a phase-locking phenomenon within the gamma band. For example, the visual cortex generated a 1/4 phase lock (1/4 subharmonic) at a driving frequency of 40 Hz. Another study demonstrated that non-linear dynamics is highly applicable to neural field models, which are driven by period stimulations.<sup>35</sup> In the present study, we demonstrate these experimental results using a theoretical model. Several  $n:m$  synchronization modes appear regularly during external periodic stimulations, which are consistent with previous findings.<sup>13,35</sup> In addition, our results are consistent with the report that the human cortex was subjected to transcranial alternating current stimulation (tACS) and responded with entrainment in alpha band.<sup>36</sup> When we increase the stimulation frequency, we find that the network responds as resonance at the integer multiples of the intrinsic frequency and the oscillation activities are strengthened. At lower stimulus frequencies, resonance and entrainment appear alternately. During resonance and entrainment, we find that the intensity of the response frequency is enhanced as well. The resonance and entrainment phenomena observed in our present research are similar to observations made during the study of non-linear oscillators. Kuki *et al.* have reported that the rat cortex yields resonance at 1 Hz with an optical stimulation of 1 Hz.<sup>10</sup> In another study, Ozen *et al.* reported the existence of cortical populations that were entrained by transcranial electric stimulations (TES) and that the specific intensity of the TES exerted influence upon the entrainment.<sup>11</sup> In the present study, we identify that the entrainment and resonance are systematically distributed in the cortex at lower stimulation frequencies.

Our theoretical analysis provides an improved understanding of network responses under periodic stimulations, while distinguishing different response regions by means of Arnold tongues. The observation of Arnold tongues in our present study provide a theoretical basis to support the existence of Arnold tongues in animal models of stimulation.<sup>37</sup> The phase-locking patterns and Arnold tongues arising from our experiments are very different when compared with previous results derived from a neural oscillator.<sup>38</sup> However, the Arnold tongues exhibited a wider width and allowed us to apply mean field theory. By comparing entrainment response described in a previous study,<sup>12</sup> it is apparent that the visual cortex generates entrainment to a stimulus over a very narrow band of stimulation frequency. Furthermore, our results confirm and

reproduce previous physiological experiments, which identified a 1:1 Arnold tongue at  $\sim 10$  Hz in EEG recordings.<sup>12</sup> We have validated that the network oscillation responds as entrainment over a more specific range of frequency variations. By comparing the entrainment response found previously in the alpha band,<sup>8</sup> we have proved that the responses are similar across different initial intrinsic frequencies. From the perspective of brain oscillations, our results provide further evidence that the mechanisms associated with lower frequencies differ from that in higher frequency counterparts.<sup>39</sup> Our study also demonstrates how responses vary with stimulation frequencies. At higher stimulus frequencies, the network responds as non-linear oscillation or oscillation suppression under different waveforms. In terms of non-linear oscillation, we observe a remarkable characteristic in that the value of the intrinsic frequency can apparently modify another. The non-linear oscillation reported in the present study is consistent with the multiplexing,<sup>14</sup> which has proved to be a valuable technique for encoding information.<sup>40</sup>

Nevertheless, there are still some limitations to our model that need to be considered when interpreting our findings. For example, we do not take synaptic plasticity into account, which may generate different response activities.<sup>41</sup> It must be clearly recognized that synaptic plasticity is neglected because of the short durations of stimulation; we consider that short stimulation durations are not sufficient to cause synaptic plasticity. In spite of a large batch of the stimulation frequencies and intensities being investigated, our work involves a limited number of waveform types and may have been limited because stimulations are administered in the form of an open loop. As a result of applying stimulation to the treatment of disease, compensation through a closed loop for individual difference<sup>15</sup> might be an effective improvement, which could contribute to distinct diseases therapy using electrical stimulation. Indeed, the Neuropace RNS System, an electrical stimulation device that targets the cortex, has recently been developed to provide clinical therapy for patients with epilepsy.<sup>42</sup> This device allows us to treat psychological diseases by discrete pulse stimulations, which provides a new perspective for the manufacture of periodic stimulus devices.

Electrical stimulations on brain oscillations are becoming a focus issue of research in delayed neural networks. This type of model could facilitate the development of other electrical stimulation-related network responses, for example, the thalamocortical network. More importantly, it is not only a meaningful supplement to the literature concerning the effect of stimulations to the neural network but also an auxiliary reference for further research studies focusing on brain stimulations' optimum selection and implementation.

## ACKNOWLEDGMENTS

This work was supported by the National Natural Science Foundation of China (NNSFC) (Grant Nos. 61701336 and 61601331) and the Tianjin Municipal Natural Science Foundation (Grant Nos. 19JCQNJC01200 and 18JCQNJC04700).

## DATA AVAILABILITY

The data that support the findings of this study are available within the article.

## REFERENCES

- <sup>1</sup>L. Glass, M. C. Mackey, and P. F. Zweifel, *Phys. Today* **42**(7), 72 (1989).
- <sup>2</sup>A. T. Winfree, *The Geometry of Biological Time* (Springer-Verlag, New York, 1980).
- <sup>3</sup>P. J. Uhlhaas and W. Singer, *Neuron* **52**, 155 (2006).
- <sup>4</sup>M. D. Fox, A. Z. Snyder, J. L. Vincent, M. Corbetta, D. C. Van Essen, and M. E. Raichle, *Proc. Natl. Acad. Sci. U.S.A.* **102**, 9673 (2005).
- <sup>5</sup>X. J. Wang, *Physiol. Rev.* **90**, 1195 (2010).
- <sup>6</sup>H. Kumar, B. W. Kim, S. Y. Song, J. S. Kim, I. S. Kim, Y. S. Kwon, S. Koppula, and D. K. Choi, *Biosci. Biotechnol. Biochem.* **76**, 1518 (2014).
- <sup>7</sup>J. Lefebvre, A. Hutt, J. F. Knebel, K. Whittingstall, and M. M. Murray, *J. Neurosci.* **35**, 2895 (2015).
- <sup>8</sup>J. Lefebvre, A. Hutt, and F. Frohlich, *eLife* **6**, 6 (2017).
- <sup>9</sup>S. Alagapan, S. L. Schmidt, J. Lefebvre, E. Hadar, H. W. Shin, and F. Frohlich, *PLoS Biol.* **14**, e1002424 (2016).
- <sup>10</sup>T. Kuki, T. Ohshiro, S. Ito, Z. G. Ji, Y. Fukazawa, Y. Matsuzaka, H. Yawo, and H. Mushiake, *Neurosci. Research.* **75**, 35 (2013).
- <sup>11</sup>S. Ozen, A. Sirota, M. A. Belluscio, C. A. Anastassiou, E. Stark, C. Koch, and G. Buzsaki, *J. Neurosci.* **30**, 11476 (2010).
- <sup>12</sup>A. Notbohm, J. Kurths, and C. S. Herrmann, *Front. Hum. Neurosci.* **10**, 10 (2016).
- <sup>13</sup>C. S. Herrmann, *Exp. Brain Res.* **137**, 346 (2001).
- <sup>14</sup>G. Thut, C. Miniusi, and J. Gross, *Curr. Biol.* **22**, R658 (2012).
- <sup>15</sup>L. Ronconi, N. A. Busch, and D. Melcher, *Sci. Rep.* **8**, 11810 (2018).
- <sup>16</sup>Spaak, F. P. De lange, and O. Jensen, *Nature* **34**, 3536 (2014).
- <sup>17</sup>N. Brunel and X. Wang, *J. Neurophysiol.* **90**, 415 (2003).
- <sup>18</sup>S. Nakata, K. Miyazaki, S. Izuhara, H. Yamaoka, and D. Tanaka, *J. Phys. Chem. A* **113**, 5876 (2009).
- <sup>19</sup>V. I. Arnol'd, *Tansl. AMS* **46**, 213 (1965).
- <sup>20</sup>M. R. Guevara, L. Glass, and A. Shrier, *Science* **214**, 1350 (1981).
- <sup>21</sup>A. Pikovsky, M. Rosenblum, J. Kurths, and R. C. Hilborn, *Am. J. Phys.* **70**, 655 (2002).
- <sup>22</sup>A. L. Barabási, R. Albert, and H. Jeong, *Physica A* **271**, 173 (1999).
- <sup>23</sup>A. Longtin, *Chaos* **11**, 1835 (2000).
- <sup>24</sup>M. McGuinness, Y. Hong, D. Galletly, and P. Larsen, *Chaos* **14**, 1 (2004).
- <sup>25</sup>K. Miyakawa and H. Isikawa, *Phys. Rev. E* **65**, 2 (2002).
- <sup>26</sup>R. Rozenfeld, J. A. Freund, A. Neiman, and L. Schimansky-Geier, *Phys. Rev. E* **64**, 051107 (2001).
- <sup>27</sup>A. Hutt, A. Mierau, and J. Lefebvre, *PLoS One* **11**, 0161488 (2016).
- <sup>28</sup>C. M. Marcus and R. M. Westervelt, *Phys. Rev. A* **39**, 347 (1989).
- <sup>29</sup>A. Hutt and L. Buhry, *J. Comput. Neurosci.* **39**, 417 (2014).
- <sup>30</sup>A. Roxin, N. Brunel, and D. Hansel, *Phys. Rev. Lett.* **94**, 238103 (2005).
- <sup>31</sup>C. Liu, C. Zhou, J. Wang, and K. A. Loparo, *IEEE Trans. Neural Syst. Rehabil. Eng.* **26**, 1649 (2018).
- <sup>32</sup>A. Dickinson, C. DiStefano, D. Senturk, and S. S. Jeste, *Euro. J. Neurosci.* **47**, 643 (2017).
- <sup>33</sup>C. R. Butson and C. C. McIntyre, *Clin. Neurophysiol.* **118**, 1889 (2007).
- <sup>34</sup>B. Zoefel, R. J. Huster, and C. S. Herrmann, *Neuroimage* **54**, 1427 (2011).
- <sup>35</sup>J. A. Roberts and P. A. Robinson, *Neuroimage* **62**, 1947 (2012).
- <sup>36</sup>R. F. Helfrich, T. R. Schneider, S. Rach, S. A. Trautmann-Lengsfeld, A. K. Engel, and C. S. Herrmann, *Curr. Biol.* **24**, 333 (2014).
- <sup>37</sup>M. M. Ali, K. K. Sellers, and F. Fröhlich, *J. Neurosci.* **33**, 11262 (2013).
- <sup>38</sup>O. Castejón and A. Guillamon, *Commun. Nonlinear Sci. Numer. Simul.* **81**, 11262 (2020).
- <sup>39</sup>E. Podvalny, N. Noy, M. Harel, S. Bickel, G. Chechik, C. E. Schroeder, A. D. Mehta, M. Tsodyks, and R. Malach, *J. Neurophysiol.* **114**, 505 (2015).
- <sup>40</sup>S. Panzeri, N. Brunel, N. K. Logothetis, and C. Kayser, *Trends Neurosci.* **33**, 111 (2010).
- <sup>41</sup>D. Strüber, S. Rach, T. Neuling, and C. S. Herrman, *Front. Cell Neurosci.* **9**, 311 (2015).
- <sup>42</sup>B. Lee, M. N. Zubair, Y. D. Marquez, D. M. Lee; L. A. Kalayjian, C. N. Heck, and C. Y. Liu, *World Neurosurg.* **84**, 719 (2015).